

Quantitative relations between nearest-neighbor persistence and slow heterogeneous dynamics in supercooled liquids

Katrianna S. Sarkar¹, Kevin A. Interiano-Alberto¹, Jack F. Douglas², and Robert S. Hoy¹

¹*Department of Physics, University of South Florida, Tampa, Florida 33620, USA and*

²*National Institute of Standards and Technology, Gaithersburg, Maryland 20899, USA**

(Dated: February 4, 2025)

Using molecular dynamics simulations of a binary Lennard-Jones model of glass-forming liquids, we examine how the decay of the normalized neighbor-persistence function $C_B(t)$, which decays from unity at short times to zero at long times as particles lose the neighbors that were present in their original first coordination shell, compares with those of other, more conventionally utilized relaxation metrics. In the strongly-non-Arrhenius temperature regime below the onset temperature T_A , we find that $C_B(t)$ can be described using the same stretched-exponential functional form that is often utilized to fit the self-intermediate scattering function $S(q, t)$ of glass-forming liquids in this regime. The ratio of the bond lifetime τ_{bond} associated with the terminal decay of $C_B(t)$ to the α -relaxation time τ_α varies appreciably and non-monotonically with T , peaking at $\tau_{\text{bond}}/\tau_\alpha \simeq 45$ at $T \simeq T_x$, where T_x is a crossover temperature separating the high- and low-temperature regimes of glass-formation. In contrast, τ_{bond} remains on the order of the overlap time τ_{ov} (the time interval over which a typical particle moves by half its diameter), and the peak time τ_χ for the susceptibility $\chi_B(t)$ associated with the spatial heterogeneity of $C_B(t)$ remains on the order of τ_{imm} (the characteristic lifetime of immobile-particle clusters), even as each of these quantities varies by roughly 5 orders of magnitude over our studied range of T . Thus, we show that $C_B(t)$ and $\chi_B(t)$ provide semi-quantitative spatially-averaged measures of the slow heterogeneous dynamics associated with the persistence of immobile-particle clusters.

I. INTRODUCTION

Numerous experimental and computational studies have shown that glass-forming liquids are dynamically heterogeneous in the sense that they possess transient regions where the relaxation dynamics can be substantially faster or slower than their spatial average [1–14]. High-mobility particles tend to form clusters with lifetimes scaling as $\tau_{\text{mob}} \sim T/D$, where T is temperature and D is the diffusion constant. Low-mobility particles tend to form clusters with lifetimes $\tau_{\text{imm}} \sim \tau_\alpha$, where τ_α is the α -relaxation time. Most studies of dynamical heterogeneity have focused on the mobile-particle clusters and the associated cooperative motion of the mobile particles in relation to understanding glass-forming liquids' temperature-dependent activation energy $E_A(T)$.

Immobile-particle clusters have also been shown to play a significant role in these liquids' dramatic dynamical slowdown. Lacevic *et al.* connected these clusters directly to α relaxation more than twenty years ago [10] by showing that they dominate the four-point position-time correlation function $\chi_4(t)$, and that the time τ_4 at which $\chi_4(t)$ is maximized tracks τ_α with decreasing T . Many studies performed since then have defined "dynamical heterogeneity" (DH) in terms of $\chi_4(t)$. DH has also been often defined in terms of the more easily calculated and experimentally determined peak in the non-Gaussian parameter $\alpha_2(t)$. Notably, the time t^* at which α_2 is maximized is a "slow β " relaxation time in the sense that it is much longer than the fast β relaxation time τ_β

governing the initial decay of $S(q, t)$, but much shorter than τ_α , in glass-forming liquids at low temperatures. Recent work has shown that t^* closely tracks that of the Johari-Goldstein relaxation time τ_{JG} [15, 16].

Starr *et al.* showed [11] that there are two distinct types of dynamic heterogeneity on these time scales [i.e., $\mathcal{O}(t^*)$ and $\mathcal{O}(\tau_\alpha)$] which are respectively associated with the mobile- and immobile-particle clusters; below, we refer to these as "fast" and "slow" DH. However, despite the advances made by a few more-recent studies [17–20], immobile-particle clusters and slow DH remain relatively poorly studied in comparison to their mobile-particle and fast counterparts, and there is clearly a need to better understand these phenomena.

In this paper, we take a different approach to characterizing the spatially-heterogeneous dynamics associated with the immobile-particle clusters. In particular, we focus on the neighbor-persistence metric $C_B(t)$, which varies smoothly from 1 to 0 as particles lose the neighbors that were present in their original first coordination shell, and captures the extent to which individual particles progressively "forget" their original local environments. $C_B(t)$ was suggested to be a natural measure of structural relaxation in supercooled liquids as far back as the work of Frenkel in the 1930s [21], and Rahman examined related quantities in some of the first molecular dynamics simulations [22], yet this metric has received surprisingly little attention over the intervening decades. This neglect can no doubt be traced to the fact that it cannot yet be experimentally measured in atomic and molecular glass-formers.

Experimental measurements of $C_B(t)$ have, however, been performed for *colloidal* glass-formers. Conrad *et al.*

* rshoy@usf.edu

showed that their solid-like, elastic response to an applied shear strain on timescales $t < \tau_{\text{solid}}$ arises from the system-spanning nature of the immobile-particle clusters on these timescales [23]. They showed that these clusters have $C_B(t < \tau_{\text{solid}}) = 1$, and further that in the glassy state, such clusters persist throughout the experimental observation window. Zhang *et al.* compared $C_B(t)$ in attractive and repulsive glasses composed of the same particles at the same packing fractions [24], and showed that the much-slower dynamics of the former systems is directly associated with their much-slower-decaying $C_B(t)$. Laurati *et al.* extended the results of Ref. [23] to mechanically-deformed systems, showing [25] that the shape of the stress-strain curves $\sigma(\gamma)$ under startup shear is intimately connected to $C_B(\gamma)$, i.e., to the fraction of particles' neighbors in the initial undeformed state which remain their neighbors at shear strain γ . Most recently, Higler *et al.* measured $C_B(t)$ in charge-stabilized colloidal suspensions with a wide range of ϕ , τ_α , τ_{bond} and coordination numbers Z [26]. They used these results to reformulate Dyre's shoving model [27, 28] for the relationship between τ_α and the cage-escape lifetime τ_{cage} (which is of order τ_{bond}) in terms of more-readily-observable particle-scale quantities.

Several additional insights have come from molecular dynamics simulations. Yamamoto and Onuki showed [29] that the time scale τ_{bond} associated with the terminal decay of $C_B(t)$ seemed to satisfy the relation $\tau_{\text{bond}} \simeq 10\tau_\alpha$, that reneighboring events become increasingly spatially heterogeneous with decreasing T , that $\tau_{\text{bond}} \propto \xi^z$ where ξ is the correlation length of such heterogeneities (i.e., the size of clusters formed by particles with few lost neighbors), and that the character of these heterogeneities is strongly affected by applied shear. Shiba *et al.* substantially extended these results, showing [30] that $\tau_{4,\text{pos}}$ was substantially shorter than the peak time $\tau_{4,\text{bond}}$ for four-point bond-breakage correlations, and claimed that this is associated with long-wavelength vibrational modes which reduce the former but not the latter. Iwashita *et al.* argued [31] that $C_B(t)$ is directly connected to the super-Arrhenius temperature dependence of fragile glass-formers' relaxation dynamics. In particular, they showed that the Maxwell time (τ_M) exceeds the average time for particles to lose *one* neighbor (τ_{LC}) for temperatures below T_c , thus identifying these single-reneighboring events as the elementary excitations in high-temperature and weakly-supercooled liquids. Most recently, Scalliet *et al.* compared the spatially-resolved $C_B[\tau_{\text{bond}}(T)]$ of supercooled liquids over a wide range of T [32]. They showed that the spatial heterogeneity of neighbor persistence increases substantially as T decreases into a regime that is more deeply supercooled than that probed by most previous simulations. In this regime, structural relaxation corresponds to transient but long-lived solid-like regions with low particle mobility and high C_B being gradually "dissolved" by liquid-like regions displaying opposite trends. This interpretation seems to agree with a wide range of recent theoretical work [33].

Taken together, these results indicate that $C_B(t)$ is an appealing relaxation metric to study because it is both experimentally accessible and simple to interpret, yet it can offer deep insights not obtainable via more-commonly studied metrics like particles' mean-squared displacement $\Delta^2(t)$ and self-intermediate scattering function $S(q, t)$. However, the *quantitative* relationships between the relaxation times associated with $C_B(t)$ and several other, more-conventionally-utilized relaxation metrics have yet to be established. In this paper, using molecular dynamics simulations of the Kob-Andersen (KA) model [34, 35], a model glass-former which has been intensively studied for three decades, we do so.

We find that for temperatures below T_A , $C_B(t)$ is well fit by the same generic double-stretched-exponential functional form

$$C_B(t) = (1 - A) \exp[-(t/\tau_{\text{fast}})^{s_{\text{fast}}}] + A \exp[-(t/\tau_{\text{slow}})^{s_{\text{slow}}}] \quad (1)$$

that is often utilized to fit $S(q, t)$ [19]. The τ_{fast} , s_{fast} and s_{slow} for $C_B(t)$ are close to those obtained by fitting the corresponding fast- β and α relaxation processes of $S(q, t)$, but the $A(T)$ are somewhat larger. Consistent with previous studies [23–26, 29–32], the characteristic neighbor lifetime τ_{slow} is substantially longer than τ_α . We also find that the ratio $\tau_{\text{slow}}/\tau_\alpha$ varies substantially with T , and peaks near T_x . On the other hand, τ_{slow} remains within a factor of order one of τ_{ov} , and τ_x remains within a factor of order one of τ_{imm} , even as each of these quantities varies by roughly 5 orders of magnitude over our studied range of T . Van Hove correlation functions evaluated at $t = \tau_x(T)$ reveal that diffusion remains strongly non-Gaussian on this timescale – increasingly so as T decreases – owing to the persistence of large immobile-particle clusters. Thus we show that $C_B(t)$ and $\chi_B(t)$ provide easily-measurable, semi-quantitative, spatially-averaged measures of the slow heterogeneous dynamics associated with immobile particles.

II. METHODS

All simulations were conducted using the High Dimensional Molecular Dynamics (**hdMD**) code [36, 37]. To capture generic supercooled-liquid behavior, we simulate the standard Kob-Andersen model [34] with a 2:1 ratio of large (A) to small (B) particles. Particles i and j interact via the truncated and shifted Lennard-Jones potential $U(r) = U_{\text{LJ}}(r) - U_{\text{LJ}}(r_c)$, where

$$U_{\text{LJ}}(r) = 4\epsilon_{ij} \left[\left(\frac{\sigma_{ij}}{r} \right)^{12} - \left(\frac{\sigma_{ij}}{r} \right)^6 \right]. \quad (2)$$

As usual [34, 35], $\epsilon_{\text{AA}} = 1.0$, $\epsilon_{\text{AB}} = 1.5$, $\epsilon_{\text{BB}} = 0.5$, $\sigma_{\text{AA}} = 1.0$, $\sigma_{\text{AB}} = 0.8$ and $\sigma_{\text{BB}} = 0.88$ in units of the system's characteristic energy and length scales, and the cutoff radius $r_c = 2.5\sigma_{ij}$.

We employ the 2:1 variant of this model rather than the historically-more-widely-studied 4:1 variant because

the latter is prone to crystallization [38]. All results reported below will be given in units of ϵ_{AA} , σ_{AA} and the time scale $\tau = \sqrt{m\sigma_{AA}^2/\epsilon_{AA}}$, where all particles have mass m . The MD timestep we employed is $dt = \tau/125$. All systems contain $N = 1.67 \times 10^5$ particles and are equilibrated at various constant temperatures $0.38 \leq T \leq 1.0$ and a small positive pressure $P = 0.01$. In real units corresponding to liquid argon, this pressure corresponds to $P \simeq 420\text{KPa}$, while our highest temperature corresponds to $T \simeq 120\text{K}^\circ$ [39, 40]. As is standard practice [35], we equilibrate systems for at least $100\tau_\alpha$ [defined using the standard criterion $S(q, \tau_\alpha) = 1/e$] for each T before beginning the measurements reported below.

Following Refs. [23–26, 29–32], we define $\mathcal{C}_B^i(t)$ as the average fraction of neighbors present in particle i 's original first coordination shell that are still present at time t . Then $C_B(t) = \langle \mathcal{C}_B^i(t) \rangle$ is the average of this quantity over all particles, and the susceptibility $\chi_B(t) = \sqrt{\langle [\mathcal{C}_B^i(t)]^2 \rangle - C_B(t)^2}$ captures the heterogeneity of this metric. Most previous studies of this quantity have defined $\mathcal{C}_B^i(t)$ as the average fraction of particle pairs with $r_{ij}(0) \leq B_1\sigma_{ij}$ that have $r_{ij}(t) \leq B_2\sigma_{ij}$, where B_1 was set to approximately correspond to the first minimum of the pair correlation functions $g_{ij}(r)$, and $B_2 \simeq 1.1B_1$. Here, particles i and j are considered neighbors at time t if $r_{ij}(t) \leq (5/4)2^{1/6}\sigma_{ij} \simeq 1.4\sigma_{ij}$ for *arbitrary* t ; this effectively sets $B_2 = B_1$.

We will compare the relaxation captured by $C_B(t)$ and $\chi_B(t)$ to several other more-conventionally-utilized relaxation metrics, specifically:

- the mean-squared displacement $\Delta^2(t) = \langle |\vec{r}_i(t) - \vec{r}_i(0)|^2 \rangle$ and non-Gaussian parameter $\alpha_2(t) = 3\langle |\vec{r}_i(t) - \vec{r}_i(0)|^4 \rangle / (5[\Delta^2(t)]^2) - 1$ [2, 35];
- the self-intermediate scattering function $S(q, t)$, evaluated for q values that are within $0.1/\sigma_{AA}$ of the peak of the static structure factor $S(q)$;
- the overlap function $f_{ov}(t)$ [10], here defined as the fraction of particles that remain within $\sigma_{ii}/2$ of their initial positions;
- the average sizes $N_{\text{mob}}(t)$ and $N_{\text{imm}}(t)$ of mobile- and immobile-particle clusters [7–11]; and
- the self part of the van Hove correlation function $G_s(r, t) = N^{-1} \sum_{i=1}^N \delta(|\vec{r}_i(t) - \vec{r}_i(0)| - r)$ [35], where $\delta(x)$ is the Dirac delta function.

To obtain a relatively simple theoretical picture, it is necessary to extract characteristic timescales from the above relaxation metrics. Here, following previous studies [7–11], we define the times t^* , τ_{mob} , and τ_{imm} as the peak times for $\alpha_2(t)$, $N_{\text{mob}}(t)$, and $N_{\text{imm}}(t)$, and similarly, we define the time τ_χ as the peak time for $\chi_B(t)$. Results for all of these quantities are time-averaged over at least ten “windows” of length $10^4\tau$ for $T > 0.42$, four windows of length $10^5\tau$ ($2.5 \times 10^5\tau$) for $0.41 \leq T \leq 0.42$

($0.39 \leq T \leq 0.40$), and two windows of length $5 \times 10^5\tau$ for $T = 0.38$.

Rigorously characterizing particles as “mobile” or “immobile” is a non-trivial exercise. Here we defined the mobile (immobile) particles as the 10% of particles that had the largest (smallest) maximal excursions from their initial positions over the time interval $[0, t]$. As in Ref. [41], this percentage was chosen because it maximized the peak *normalized* average mobile-particle cluster size, i.e. the maximal $N_{\text{mob}}(t)/N_{\text{rand}}$, where N_{rand} is the average size of clusters formed by randomly selected particles.

Note that the $f_{ov}(t)$ defined above is the *self*-overlap function, i.e.

$$f_{ov}^{\text{self}}(t) = \frac{1}{N} \sum_{i=1}^N \Theta[\sigma_{ii}/2 - |\vec{r}_i(t) - \vec{r}_i(0)|], \quad (3)$$

where Θ is the Heaviside step function. Ref. [10] showed that the susceptibility $\chi_4(t) = \langle [f_{ov}^{\text{mut}}(t)]^2 \rangle - \langle f_{ov}^{\text{mut}}(t) \rangle^2$ of the *mutual* overlap function $f_{ov}^{\text{mut}}(t) = Q/N$, where

$$Q = \frac{1}{N} \sum_{i=1}^N \sum_{j=1}^N \Theta[a\sigma_{ij} - |\vec{r}_j(t) - \vec{r}_i(0)|] \quad (4)$$

is the integral of the four-point position/time correlation function $\mathcal{G}[\vec{r}_i(0), \vec{r}_j(t), \vec{r}_k(0), \vec{r}_l(t)]$ over all $[\vec{r}_i(0), \vec{r}_j(t), \vec{r}_k(0), \vec{r}_l(t)]$. It also showed that $f_{ov}^{\text{self}}(t)$ provides the dominant contribution to $f_{ov}^{\text{mut}}(t)$, and that choosing $a = 0.3$ maximizes the heights $\chi_4^{\text{max}}(T)$ of the peaks of $\chi_4(t)$. Many studies which have used this cutoff have *defined* DH in terms of $\chi_4(t)$. Moreover, it has been argued that $\chi_4^{\text{max}}(T)$ scales with the characteristic correlation lengths $\xi_4(T)$ of DH over time scales $t \sim \tau_\alpha$ as $\chi_4^{\text{max}} \sim \xi_4^{2-\epsilon}$, where the scaling exponent is material-dependent [42–45]. Below, we will show that our alternative choice (i.e. $a = 1/2$) allows us to more effectively characterize systems’ slow DH on time scales $t \gg \tau_\alpha$.

III. RESULTS

A. Qualitative characterization of eight different structural-relaxation metrics

Figure 1 summarizes the T - and t -dependence for five of the metrics discussed above. All results shown in panels 1a-1b are similar to those reported in many previous studies [1, 35], but since they set the stage for what will follow, we discuss them in some detail here. Plateaus in both $\Delta^2(t)$ and $S(q, t)$ begin to form as T drops below the onset temperature for non-Arrhenius relaxation, $T_A \simeq 0.64$; this corresponds to the emergence of a distinct fast β relaxation process with a nearly T -independent relaxation time τ_β and a slow α relaxation process with a strongly T -dependent τ_α . The separation between these timescales upon further cooling exhibits a sharp increase as T drops below $T_x \simeq 0.45$. We will discuss how these estimates of T_A and T_x were obtained in Section III B.

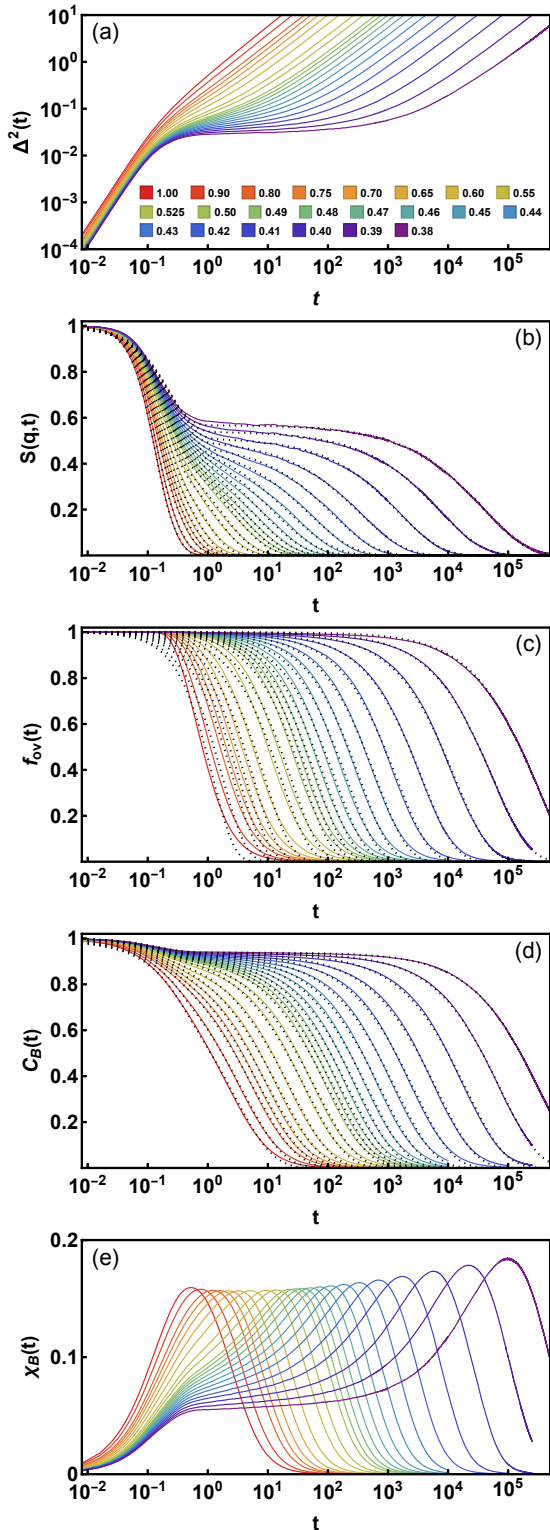


FIG. 1. Three traditional measures of single-particle dynamics compared to two measures of nearest-neighbor persistence. Panels (a-e) respectively show $\Delta^2(t)$, $S(q,t)$, $f_{ov}(t)$, $C_B(t)$ and $\chi_B(t)$ for systems over the temperature range $0.38 \leq T \leq 1.0$. The color legend in panel (a) shows each T value. Dotted curves in panels (b-d) show fits to Eqs. 5-7.

There are two notable differences between the behavior of $\Delta^2(t)$ and $S(q,t)$ and that of $f_{ov}(t)$ (panel 1c). First, unlike the former metrics, $f_{ov}(t)$ exhibits single-step decay for all T . Second, in contrast to previous studies which employed $a = 0.3$ (Sec. II) and found that the characteristic relaxation time τ_{ov} defined by $f_{ov}(\tau_{ov}) = 1/e$ was of order τ_α , the plateaus in $f_{ov}(t)$ shown here extend to substantially longer times, indicating a $\tau_{ov} \gg \tau_\alpha$. In other words, throughout the plateau regimes suggested by measurement of particles' mean-squared displacement and self-intermediate scattering function, very few particles have moved by even half their diameter. This is not surprising given that $r_{cage} \ll \sigma_{ii}/2$, but it does raise the question of how to visualize the physical relaxation process associated with these larger τ_{ov} .

To begin answering this question, we now look at these systems' $C_B(t)$ (panel 1d). At high and intermediate T , the $C_B(t)$ exhibit smooth, apparently-single-time-scale decays similar to those reported in previous studies [23–26, 29–32]. For $T \lesssim T_x$, however, the $C_B(t)$ exhibit plateaus which lengthen rapidly with decreasing T , much like those for $\Delta^2(t)$, $S(q,t)$ and $f_{ov}(t)$. These plateaus have not been previously reported because Refs. [23–26, 29–32] employed B_2 which were well above B_1 (Sec. II), whereas here we employ $B_2 = B_1$. This difference introduces an additional relaxation mechanism in our $C_B(t)$ that was not captured in previous studies: specifically, particle-pair distances evolving back and forth across the above-mentioned $r_{ij} \leq (5/4)2^{1/6}\sigma_{ij}$ neighboring cutoff. Below, we will argue that this mechanism is associated with fast β -relaxation.

Beyond their plateau regimes, the decays of $C_B(t)$ and $f_{ov}(t)$ closely track each other, indicating that particles losing their neighbors roughly corresponds to them moving by more than half their diameters. This is not surprising from a qualitative point of view, but as we will show below, it leads to an interpretation of the connection of $C_B(t)$ to other measures of heterogeneous relaxation dynamics that is substantially different from those developed in previous studies which employed $a = 0.3$ [10, 29–32]. Note that panels 1b-1d also show fits of $S(q,t)$, $f_{ov}(t)$, and $C_B(t)$ to Eq. 1, but before discussing these, we will turn our attention to measures of heterogeneous dynamics in these systems.

At the same high T for which $S(q,t)$ and $C_B(t)$ exhibit single-time-scale relaxation, $\chi_B(t)$ takes on an approximately log-normal form (panel 1e). As T drops below T_x , clear plateaus of $\chi_B(t)$ that mirror those of $C_B(t)$ emerge. Beyond the plateau regime, the heights $\chi_B^{\max}(T)$ of the peaks in the $\chi_B(t)$ curves begin increasing with decreasing T . Note that the gradual emergence of two-time-scale decay of $S(q,t)$ and $C_B(t)$, as T decreases, coincides with (1) a decrease in the maximal slopes $d\chi_B/d[\ln(t)]$, (2) a reduction of the χ_B values at which the inflection points in the $\chi_B(t)$ curves occur, and (3) a rapid increase of τ_χ . As we will discuss further below, all of these trends indicate that $C_B(t)$ and $\chi_B(t)$ as defined in this paper can serve as useful *spatially-averaged* measures of the slow

DH associated with the relatively immobile particles.

Figure 2 shows results for three more metrics which are often employed to characterize dynamical heterogeneity. In all panels, the trends with decreasing T are consistent with many previous studies [7–11]. More specifically, the maximum values of $\alpha_2(t)$, $N_{\text{mob}}(t)$, and $N_{\text{imm}}(t)$, and the times t^* , τ_{mob} , and τ_{imm} at which these maxima occur each increase rapidly with decreasing T for $T \lesssim T_x$. The increasing separation between fast DH timescales like t^* and τ_{mob} and slow DH timescales like τ_{imm} has been discussed extensively [1–3, 11]. However, as mentioned in the Introduction, while most previous studies have focused on assigning a physical meaning to the fast timescales (e.g., showing that $t^* \sim \tau_{\text{mob}} \sim T/D$ [7–11]), here we will focus on the relatively slow particles. More specifically, we will quantitatively relate τ_{imm} , which measures the characteristic lifetime of immobile regions whose characteristic size grows very rapidly with increasing T [10, 11], to *local, single-length-scale* neighbor-persistence timescales obtainable from measurements of $C_B(t)$ and $\chi_B(T)$.

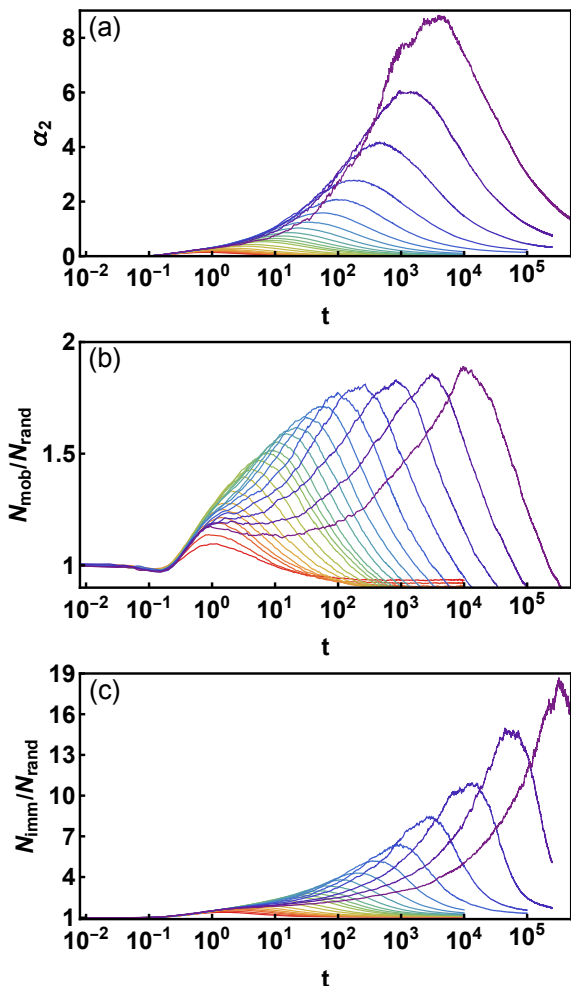


FIG. 2. Traditional measures of dynamical heterogeneity. Panels (a-c) respectively show $\alpha_2(t)$, $N_{\text{mob}}(t)$, and $N_{\text{imm}}(t)$ for all systems; colors are the same as in Fig. 1.

B. Quantitative comparison of seven different relaxation times

Next, we fit the data shown in Fig. 1(a-c) to the common, non-exponential functional form discussed above (Eq. 1). To avoid ambiguity in the following discussion, we will first rewrite Eq. 1 in ways that are specific to the three quantities of interest. For the self-intermediate scattering function, we rewrite it as [19, 46, 47]

$$S(q, t) = (1 - A_S) \exp[-(t/\tau_\beta)^{s_\beta}] + A_S \exp[-(t/\tau_\alpha)^{s_\alpha}], \quad (5)$$

where A_S is the well-known “non-ergodicity” parameter [48], τ_β and τ_α are the fast- β and α relaxation times, and s_β , s_α are the associated exponents quantifying the degree of deviation from exponential relaxation. This form should accurately describe $S(q, t)$ for temperatures $T < T_A$, where $\tau_\alpha \gg \tau_\beta$.

For the overlap function, the fact that $f_{\text{ov}}(t) \equiv 1$ until particles begin moving at last half their diameters away from their initial positions allows us to set $A = 1$ and therefore to reduce the number of parameters in Eq. 1 from five to two. Thus, we rewrite Eq. 1 as

$$f_{\text{ov}}(t) \simeq \exp[-(t/\tau_{\text{ov}})^{s_{\text{ov}}}], \quad (6)$$

where τ_{ov} is the terminal relaxation time associated with this relaxation process and s_{ov} is the associated stretching exponent. The poor agreement of this approximate functional form with simulation results for $t \lesssim 10^0$ [Fig. 1(c)] is not a major concern for the purposes of this study because we are focusing on the terminal relaxation. Note that this issue could have been avoided by using $f_{\text{ov}}^{\text{mut}}(t)$ [Eq. 4], which exhibits a two-step decay [10] and can be fit using the same functional form as Eqs. 1 and 5.

Finally, for the neighbor-persistence function, we rewrite Eq. 1 as

$$C_B(t) = (1 - A_C) \exp[-(t/\tau_{\text{fast}})^{s_{\text{fast}}}] + A_C \exp[-(t/\tau_{\text{bond}})^{s_{\text{bond}}}], \quad (7)$$

Here A_C plays a role similar to the ergodicity parameter, the fast-relaxation parameters τ_{fast} and s_{fast} capture the behavior of $C_B(t)$ ’s abovementioned fast decay mode, and τ_{bond} , s_{bond} are the average nearest-neighbor lifetime and associated stretching exponent discussed in Refs. [29, 30]. Our best-fit values of the parameters in Eqs. 5-7, along with uncertainty estimates, are given in the Appendix.

Before proceeding further, we define both the onset temperature T_A and the crossover temperature T_x . These temperatures are typically estimated using the α relaxation times. T_A has traditionally been defined [35] as the temperature below which τ_α increases super-Arrheniusly with decreasing T and substantial dynamical heterogeneity emerges [49]. A precise criterion was given in Ref. [40], which showed that defining T_A as the highest temperature for which $\tau_\alpha(T)$ is 1% above its high- T Arrhenius fit value allows $\tau_\alpha(T_A)$ to be identified with the “caging onset time” and to serve as a reference time scale for structural relaxation and diffusion.

T_x has traditionally been defined [35] with the critical temperature T_c of mode-coupling theory, by fitting $\tau_\alpha(T)$ to its predicted power-law divergence $\tau_\alpha(T) \sim (T_c - T)^{-\gamma}$ [50], over a limited temperature range. Values of T_c obtained in this fashion depend strongly on the choice of temperature range over which $\tau_\alpha(T)$ is fit to this functional form [51], however, and $\tau_\alpha(T)$ does not actually diverge at the fitted T_c . An alternative estimate of the crossover temperature T_x can be obtained by finding the maximum of $d^2[\ln(\tau_\alpha)]/d(1/T)^2$ on a Stickel plot [52], or (roughly equivalently for systems exhibiting a fragile-to-strong crossover [53]) by finding the intersection of the high- T and low- T Arrhenius fits to $\tau_\alpha(T)$ [54]. This definition of T_x is comparable to the crossover temperature defined in the Generalized Entropy Theory (GET) [55] that separates the high- and low-temperature regimes of glass formation. Note that the GET also predicts a power-law variation of τ_α over a limited T range and predicts the precise value of this crossover temperature.

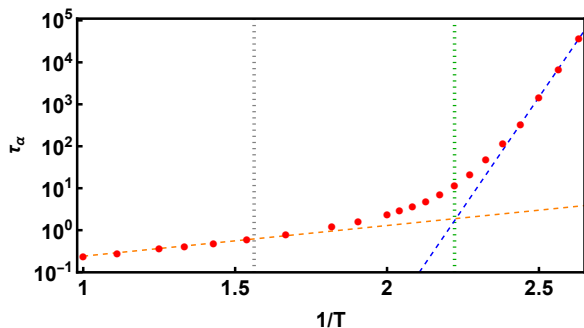


FIG. 3. α relaxation times obtained by fitting $S(q, t)$ to Eq. 5. Dashed lines show fits of $\tau_\alpha(T)$ to the Arrhenius prediction $\tau_{\text{Arr}}(T) = \tau_0 \exp(E_{\text{Arr}}/T)$; the high- and low- T fits intersect at $T = T_x \simeq 0.45$. Dotted lines indicate $1/T_A$ and $1/T_x$.

Figure 3 shows the $\tau_\alpha(T)$ obtained from fitting our $S(q, t)$ data to Eq. 5. The data are consistent with a previous study of the KA model’s 2:1 variant at $P = 0$ [56], and all trends are similar to those observed in many previous studies. Here we emphasize two key features. First, τ_α increases by more than five orders of magnitude (from $\simeq 0.24$ to $\simeq 3.7 \times 10^4$) as T decreases from 1.0 to 0.38. Second, the procedures described above [40, 54] respectively yield $T_A \simeq 0.64$ and $T_x \simeq 0.45$; for reference, $\tau_\alpha(T_A) \simeq 0.62$ and $\tau_\alpha(T_x) \simeq 12$.

We will show below that this estimate of T_x closely corresponds to two other characteristic features in the temperature dependence of our systems’ relaxation dynamics. We also remark that the characteristic temperatures of the Kob-Andersen model depend strongly on pressure [40], and this should be borne in mind when comparing our results to those from the many previous simulations of the Kob-Andersen model that employ constant density. The values that we find for T_A and T_x are roughly consistent with corresponding estimates for the 4:1 KA model when P is small.

Detailed results for A_S , A_C , τ_β , τ_{fast} , s_β , s_α , s_{ov} , s_{fast}

and s_{bond} are given in the Appendix. Here we emphasize that for all temperatures which are low enough for relaxation to have a clearly-two-step character (i.e., $T \leq T_A$), τ_{fast} and s_{fast} are respectively close to τ_β and s_β . This shows that the initial stage of $C_B(t)$ ’s decay is closely associated with the fast β relaxation [1]. We also find that $s_{\text{bond}} \simeq s_\alpha$ for $T \lesssim 0.5$, suggesting that neighbor persistence and α relaxation are similarly heterogeneous in this regime.

Figure 4 shows results for the seven other relaxation times defined above. Panel 4a compares the $\tau_\alpha(T)$ obtained by fitting $S(q, t)$ to Eq. 5 to the two measures of fast DH shown in Fig. 2(a-b). All results are similar to those reported in multiple previous studies [7–11]. The main features we wish to highlight here are that: (1) t^* and τ_{mob} are essentially identical on the scale of the plot, except at the lowest T , where τ_{mob} is clearly the larger of the two; and (2) both of these times grow much more slowly with decreasing T than $\tau_\alpha(T)$.

Panel 4b compares these $\tau_\alpha(T)$ to τ_{imm} [Fig. 2(d)], τ_χ , the τ_{ov} obtained by fitting $f_{\text{ov}}(t)$ to Eq. 6, and the τ_{bond} obtained by fitting the $C_B(t)$ data to Eq. 7. Three trends are apparent from examining the relations between these quantities. First, as previously reported in Refs. [29–32], τ_α remains well below τ_{bond} for all T . Second, in contrast to the results shown in panel 4a, τ_α also remains well below the other three timescales for all T , and for high and intermediate temperatures, τ_α grows slower with decreasing T . Third, τ_{bond} is substantially larger than τ_{ov} at high T , but these times converge as T decreases, consistent with the geometrically-intuitive notion that particles losing their original neighbors corresponds to them moving by roughly half their diameter away from their initial positions *when caging is strong and motion is hopping-dominated*, i.e., at low T .

Panels 4c and 4d, which respectively show the ratios of τ_{bond} and τ_χ to the other timescales, illustrate the above-mentioned relationships in more detail. Again, three key trends are apparent. First, the ratios of τ_{bond} and τ_χ to the fast-DH timescales t^* and τ_{mob} increase steadily with decreasing T . The ratio of τ_{bond} to these timescales reaches $\mathcal{O}(10^2)$ at our lowest $T = 0.38$, showing that the much-discussed decoupling [1, 2] of the fast and slow relaxation timescales in supercooled liquids also occurs for timescales associated with neighbor persistence. Second, $0.3 < \tau_\chi/\tau_{\text{imm}} < 1.2$ and $1.0 < \tau_{\text{bond}}/\tau_{\text{imm}} < 5.2$ over the entire range of T , even though all three quantities increase by 5 orders of magnitude as T decreases from 1.0 to 0.38. This shows that $C_B(t)$ and $\chi_B(t)$ are closely associated with the immobile-particle clusters.

A third trend evident in these panels is that the ratios $\tau_{\text{bond}}/\tau_\alpha$ and $\tau_{\text{bond}}/\tau_{\text{imm}}$ closely track each other, and both appear to peak at $T \simeq 0.48$, which is only slightly above our estimated T_x . Previous studies have established that $\tau_{\text{imm}} \sim \tau_\alpha$ [10, 11]. We find that the ratio of these two quantities varies over the narrow range $6.5 < \tau_{\text{imm}}/\tau_\alpha < 11.5$ despite the fact that each quantity varies by 5 orders of magnitude over our studied range

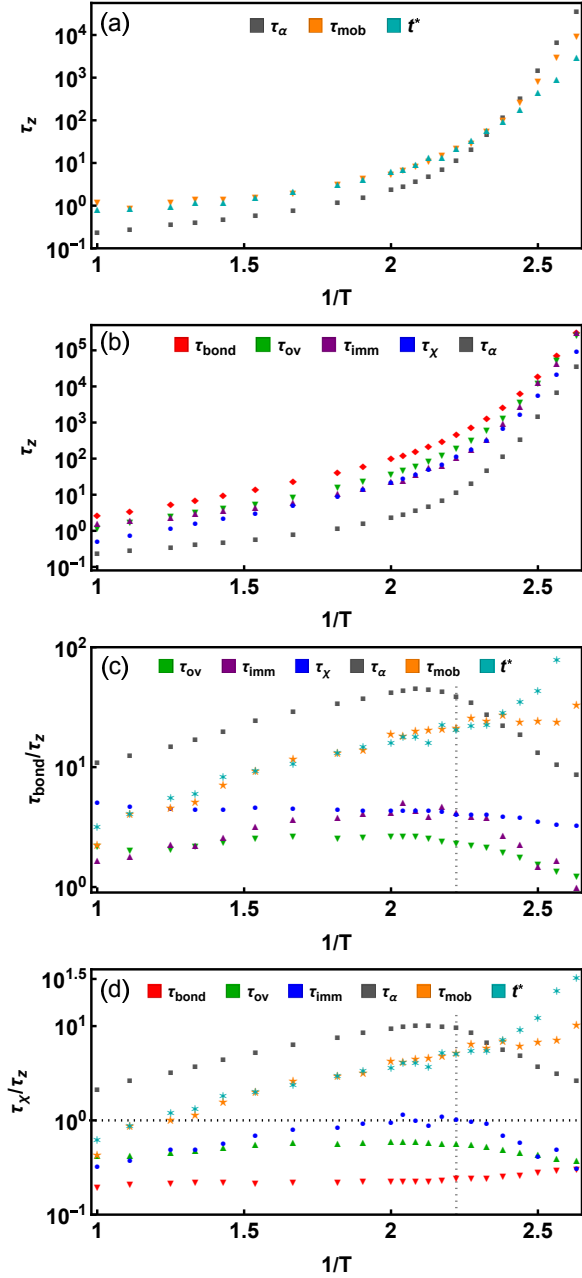


FIG. 4. Comparison of seven different relaxation times τ_z in 2:1 KA liquids at $P = .01$. Panels (a-b) respectively compare the relaxation times associated with $C_B(t)$ and $S(q, t)$ to those associated with other metrics for fast and slow DH, while panels (c-d) respectively show the ratios of τ_{bond} and τ_χ to these times. Vertical dotted lines in panels (c-d) show $1/T_x$, and the horizontal dotted line in panel (d) shows $\tau_\chi/\tau_z = 1$.

of T . The peaks in $\tau_{\text{bond}}/\tau_{\text{imm}}$ and $\tau_{\text{bond}}/\tau_\alpha$ at $T \simeq T_x$ point to a secondary effect that is not captured by the abovementioned connections between τ_{bond} , τ_χ and τ_{imm} .

We believe that these peaks are directly associated with *decoupling*. Decoupling in an experimental context is often associated with the “breakdown” of the Stokes-Einstein scaling relationship $D \sim \eta^{-1}$ between fluids’

mass diffusion coefficient D and shear viscosity η [1]. This breakdown arises when the relatively long timescales associated with the immobile particles and structural relaxation (e.g., τ_χ and τ_α) start growing faster than the shorter timescales associated with the mobile particles and the average rate of molecular diffusion (e.g., τ_{mob} and t^*) with decreasing T . It is qualitatively described by the “fractional” Stokes Einstein relation [57], a general power-law scaling relation $t^* \sim \tau_\alpha^{1-\zeta}$ between these characteristic times, where $\zeta < 1$ is the exponent characterizing the strength of decoupling [11]. Recent work [16, 40, 58, 59] has also connected decoupling directly to τ_β , and related this basic molecular timescale to the much longer timescales t^* and τ_α which are in turn connected directly to the decoupling of D and η . In particular, Yuan *et al.* found that the 4:1 KA model obeys $t^*/\tau_\beta \sim (\tau_\alpha/\tau_\beta)^{1-\zeta}$, with $\zeta \simeq 0.26$, for a wide range of densities and pressures [40, 59].

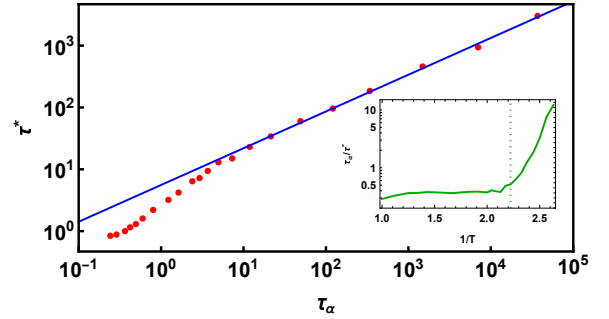


FIG. 5. Coincidence of the peaks in $\tau_{\text{bond}}/\tau_\alpha$ and $\tau_{\text{bond}}/\tau_{\text{imm}}$ with the onset of strong decoupling. The solid line shows a fit of the data to $t^* \sim \tau_\alpha^{1-\zeta}$ (with $\zeta = 0.41$). In the inset, the curve shows τ_α/t^* for the same dataset shown in Fig. 4, while the vertical dotted line shows $1/T_x$.

As shown in Figure 5, both the crossover to $t^* \sim \tau_\alpha^{1-\zeta}$ scaling and the onset of rapidly increasing τ_α/t^* occur at $T \simeq T_x \simeq 0.45$ in our systems. Thus, the peaks in $\tau_{\text{bond}}/\tau_\alpha$ and $\tau_{\text{bond}}/\tau_{\text{imm}}$, and the subsequent decrease of these quantities with decreasing T , can be interpreted as part of the crossover to the low-temperature ($T < T_x$) regime of glass-formation [55]. The $\zeta \simeq 0.41$ value reported here is larger than that reported in Ref. [40] because our measurements of τ_α and t^* were obtained from the $S(q, t)$ and $\alpha_2(t)$ of *all* particles, whereas those performed in Ref. [40] included the dynamics of *A* particles only, as is the common practice [35]. Adopting this practice for our systems decreases ζ to $\simeq 0.30$ and shifts the crossover to $t^* \sim \tau_\alpha^{1-\zeta}$ scaling upwards, to $T \simeq 0.50$. Here we prefer to use the values associated with all particles because metrics of heterogeneous dynamics such as τ_{bond} , τ_{mob} and τ_{imm} necessarily include all particles. However, the slightly higher estimate (i.e., $T \simeq 0.50$) is also close to the peaks in $\tau_{\text{bond}}/\tau_\alpha$ and $\tau_{\text{bond}}/\tau_{\text{imm}}$. Finally, it must be noted that the P value we have chosen to employ (i.e., $P = 0.01$) is exceptionally low in comparison to most previous studies, and the choice of P apparently

influences the point where the power law scaling sets in. This phenomenon requires further study.

C. Connections to heterogeneous caging

Next, we connect the above results to heterogeneous *caging*. In three spatial dimensions, the probability $P(r, t)$ that a particle has moved a distance r away from its initial position after a time t is $P(r, t) = G_s(r, t)/(4\pi r^2)$. According to Einstein's theory of Brownian motion, $P(r, t)$ is Gaussian, and the central limit theorem *requires* that $P(r, t)$ becomes Gaussian after sufficiently long times for a fluid in thermal equilibrium. At shorter times, however, $P(r, t)$ is clearly non-Gaussian in a wide variety of glass-forming liquids, including particulate systems near their glass and jamming transitions [60, 61].

Exponential tails of form $P_E(r, t) \propto \exp[-r/\Lambda]$, where Λ increases slowly with t [61–64], have been claimed to be universal in systems where motion is hopping-dominated [61, 64]. The slow crossovers to Gaussian $P(r, t)$ have been directly associated [62, 63] with the approach to ergodicity. The exponential tails $P_E(r, t) \propto \exp[-r/\Lambda]$ are known to correspond to the *mobile* particles [61, 64]. In contrast, the connection of non-Gaussian $P(r, t)$ on timescales $t \gg \tau_\alpha$ to *immobile* particles and slow DH remains rather poorly characterized. In particular, $P(r, t)$ has not yet been directly related to $C_B(t)$ or the other measures of slow DH discussed above. Here we do so.

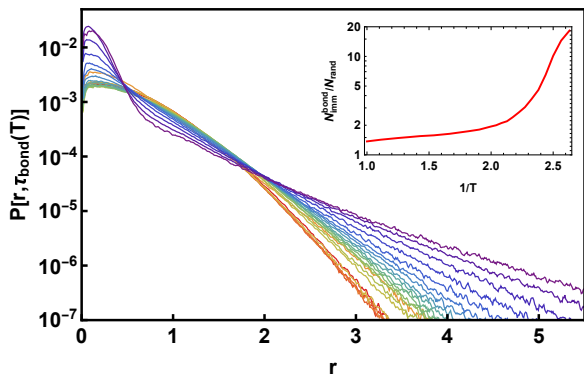


FIG. 6. Normalized van Hove correlation functions evaluated at the $t = \tau_{\text{bond}}(T)$ obtained by fitting $C_B(t)$ to Eq. 7. The inset shows the $N_{\text{imm}}^{\text{peak}}[\tau_{\text{bond}}(T)]/N_{\text{rand}}$ from Fig. 2(c). Colors are the same as in Fig. 1.

Figure 6 shows that $P[r, \tau_{\text{bond}}(T)]$ becomes increasingly non-Gaussian as T decreases. Two notable trends are evident. First, the lengths of the exponential tails in $P(r)$ increase rapidly with decreasing T for all $T \lesssim 0.7$. Since these tails correspond to the mobile particles, this trend reflects the increasing τ_{bond}/t^* and $\tau_{\text{bond}}/\tau_{\text{mob}}$ shown in Fig. 4(c). Second, a prominent low- r peak develops as T drops below T_x . This is directly associated with the above-mentioned increasing peak height of

$\chi_B(t)$ [Fig. 1(e)], and more generally, with the increasing spatial contrast between liquid-like mobile and solid-like immobile regions discussed in Ref. [32]. The inset shows that it is also directly associated with the persistence of increasingly-large immobile-particle clusters.

Our results indicate that diffusion does not become fully Gaussian (and ergodicity is not recovered) until t is several times larger than $t = \tau_{\text{bond}}(T)$. While this conclusion is consistent with those of Refs. [23–26, 29–32], it had not previously been supported so decisively. Moreover, since $\tau_{\text{bond}} > 10\tau_\alpha$ for all T and indeed $\tau_{\text{bond}} > 40\tau_\alpha$ for $T \simeq T_x$, our results also provide a microscopic justification for the commonly-employed $t_{\text{eq}} > 100\tau_\alpha$ criterion for equilibrating supercooled liquids [35].

To illustrate the connections between the various trends discussed above, Figure 7 shows snapshots of the largest immobile-particle cluster at $t = \tau_\chi(T)$ for $T = 0.38$. This cluster contains 14,682 atoms, i.e. over 85% of all the $N/10$ immobile particles present in the system. It exhibits a fractal structure familiar from previous studies examining the moderately-supercooled regime [11, 17, 32, 65], and percolates along all three directions. The left image color-codes particles by their *maximal* displacements over the interval $0 < t \leq \tau_\chi$, while the right image color-codes particles by their $C_B(\tau_\chi)$. The color variations in the two images match up well, i.e. the least-mobile particles in the left image appear to correspond closely to the highest- C_B particles in the right image. More specifically, more than 99% of the atoms in this cluster have $\Delta(\tau_\chi) \equiv \langle |\vec{r}_i(\tau_\chi) - \vec{r}_i(0)| \rangle \leq 0.3$ and $C_B(\tau_\chi) \geq 0.75$. Thus the low- r peak in $P(r, t)$ (Fig. 6) is dominated by the atoms in this cluster.

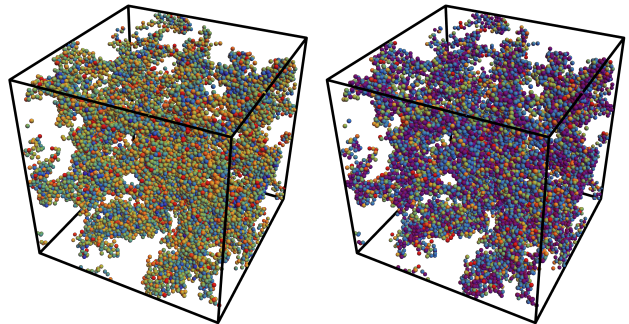


FIG. 7. Snapshots of the largest (14682-atom) immobile cluster at $t = \tau_\chi(T)$ for $T = 0.38$. The left image color-codes particles by their maximal displacements Δ_{max} over the interval $0 < t \leq \tau_\chi$, while the right image color-codes particles by their $C_B(\tau_\chi)$. Colors vary from purple to red for $0 \leq d_{\text{max}} \leq 0.3$ and $1 \geq C_B(\tau_\chi) \geq 0.75$, respectively.

IV. DISCUSSION AND CONCLUSIONS

Understanding the dramatic slowdown of supercooled liquids' dynamics with decreasing temperature T is severely hampered by the fact that only a few of the relax-

ation metrics considered in theories and simulations are readily measurable in experiments. For example, measurements of the diffusion constant D and alpha relaxation time τ_α can be used to investigate characteristic aspects of glassy dynamics such as the breakdown of the Stokes-Einstein relation ($D\tau_\alpha = \text{constant}$) [1, 2]. Modern probe-molecule-reorientation experiments can provide a great deal of information about dynamical heterogeneity by characterizing how the exponent β associated with stretched-exponential relaxation functions of the common form $F(t) \sim \exp[-(t/\tau)^\beta]$ depends on the length and time scales over which relaxation is probed [13, 14]. However, such phenomenological observational trends do not provide a clear physical understanding of the molecular origin of these phenomena.

Here we have shown that a simple neighbor-persistence metric $C_B(t)$, which is readily experimentally accessible in colloidal glassformers [23–26], can help resolve this issue. In fact, $C_B(t)$ and its variance $\chi_B(t)$ provide near-quantitative metrics for the slow, spatially-heterogeneous dynamics which occur over timescales from 10 to $100\tau_\alpha$ and length scales far above those of individual atoms’ first coordination shells. More specifically, $C_B(t)$ and $\chi_B(t)$ provide spatially-averaged measures of the dynamics associated with immobile-particle clusters.

We showed that the peak time τ_χ for the susceptibility $\chi_B(t)$ associated with the spatial heterogeneity defined by $C_B(t)$ remains on the order of τ_{imm} (the characteristic lifetime of immobile-particle clusters), even as both of these quantities varied by roughly 5 orders of magnitude over our studied range of T . Examining the Van Hove correlation functions evaluated at $t = \tau_\chi(T)$ reveal that diffusion remains strongly non-Gaussian on this timescale – increasingly so as T decreases – owing to the persistence of large immobile-particle clusters over this timescale.

Similarly, we showed that the bond lifetime τ_{bond} associated with the terminal decay of $C_B(t)$ remains on the order of the “overlap time” τ_{ov} over which a typical particle moves by at least half its diameter away from its initial position, even as both of these quantities (much like τ_χ and τ_{imm}) varied by roughly 5 orders of magnitude. A key step in making this connection was our decision to use $a = 1/2$ in Eqs. 3-4, rather than the smaller value ($a = 0.3$) used in previous studies relating neighbor persistence to heterogeneous dynamics. Specifically, choosing $a = 1/2$ made $\tau_{\text{ov}} \simeq \tau_{\text{bond}}$, a relationship which is qualitatively different than the $\tau_{\text{ov}} \simeq \tau_\alpha \ll \tau_{\text{bond}}$ relationship that is observed when $a = 0.3$ [10, 29, 30].

Finally we showed that the ratio $\tau_{\text{bond}}/\tau_\alpha$ varies substantially and non-monotonically with T , peaking at $T \simeq T_x$. Recall that τ_α starts to increase sharply, and decoupling of fast and slow relaxation processes occurs, as T drops below the crossover temperature T_x [1, 2]. We believe that $\tau_{\text{bond}}/\tau_\alpha$ decreases with decreasing T for $T < T_x$ because both timescales are controlled primarily by the immobile-particle clusters. Followup studies that probe the more-deeply-supercooled regime are needed to test this hypothesis more decisively, but one tentative

piece of evidence for it is the fact that $s_{\text{bond}} \simeq s_\alpha$ in this temperature regime [Fig. 8(c)].

We conclude by speculating on how one might further interpret the timescale τ_{bond} . One intriguing possibility is that it provides an easily-accessible estimate of the “exchange time” τ_{ex} [5, 11, 13, 14, 66], which is the average time it takes for a “fast” (high-mobility) region to become “slow” (low-mobility) and vice versa. While τ_{ex} is conceptually straightforward, mapping it onto a specific observable which can be measured in simulations, let alone experiments, has proven challenging [14]. Traditionally it has been estimated using four-point correlation functions [29, 45, 66–68]. A recently published simulation study used a novel theoretical approach to calculate τ_{ex} from *two*-point spatiotemporal correlations of local relaxation rates $\gamma(\vec{r}, t)$ [69], but associating τ_{ex} with τ_{bond} would provide an even simpler measure of τ_{ex} that directly associates it with the timescale over which particles forget their local environments. It would be interesting to attempt to do so.

We thank Ludovic Berthier and Camille Scalliet for helpful discussions. This material is based upon work supported by the National Science Foundation under Grant Nos. DMR-2026271 and DMR-2419261.

V. APPENDIX

Additional results obtained from fitting the $S(q, t)$, $f_{\text{ov}}(t)$ and $C_B(t)$ data to Eqs. 5-7 are shown in Figure 8. Panel 8a shows our results for the $A(T)$. Fig. 1 had already made it clear that the $A(T)$ are much larger for $C_B(T)$ than they are for $S(q, t)$, but this data shows that they are also both nearly T -independent for $T \gtrsim 0.7$. For larger T , these data are less reliable because the nearly-single-step nature of the decays of $S(q, t)$ and $C_B(t)$ produces ambiguities in fits of these data to Eqs. 5 and 7.

Panel 8b shows that the temperature dependence of the “beta” relaxation times τ_β and τ_{fast} is much weaker than it is for slow timescales like τ_α and τ_{bond} . This is expected from the well-known weak temperature dependence of β relaxation [1]. In stark contrast to results for the various τ_{slow} , the ratio $\tau_{\text{fast}}/\tau_\beta$ remains nearly constant (and of order one) for all T for which the decay of $S(q, t)$ and $C_B(t)$ clearly has a two-step character, i.e., for all $T \lesssim T_A$. It would be interesting to investigate this fast decay mode further, as the dynamics of β relaxation are quite complex and remain a topic of active study [70–72]. Note that as mentioned above, in contrast to previous studies [29–32], here we did not suppress the fast decay mode of $C_B(t)$ by including a “padding” of the distance cutoff for particles to be considered neighbors.

Panel 8c shows our results for the fast and slow stretching exponents. s_{fast} tracks and is comparable to the exponent s_β over the entire range of T , further supporting our identification of the fast decay mode of $C_B(t)$ with β relaxation. Note that our results for $s_\beta(T)$ are in qualitative agreement with several previous studies [70–73].

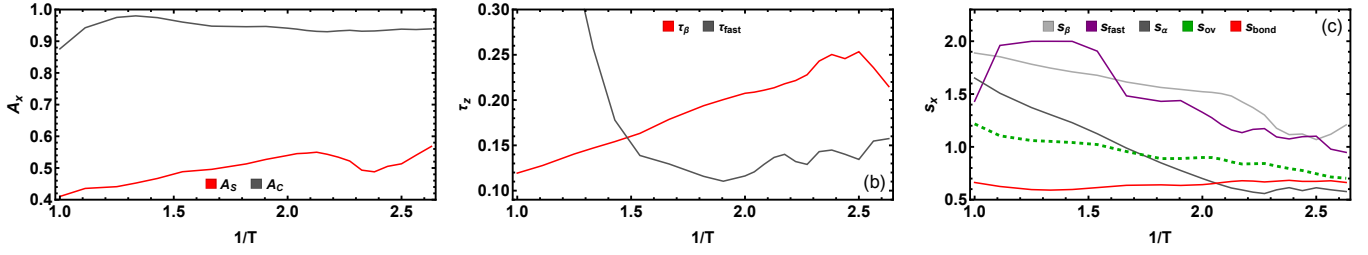


FIG. 8. A_S , A_C , τ_β , τ_{fast} , s_{fast} , s_β , s_{ov} , and s_{slow} values obtained by fitting simulation data for $S(q, t)$, $f_{ov}(t)$, and $C_B(t)$ to Eqs. 5-7. Statistical uncertainties for these parameters are comparable to the scatter of the plotted data.

TABLE I. Equilibrium densities $\rho = N/V$ and best-fit values for the seven relaxation times discussed in Sec. IIIB. All times are given to two significant figures because the estimated statistical uncertainties on most quantities are of order 1%. The uncertainties for τ_{mob} and τ_{imm} are larger for $T \leq 0.4$ owing to the limited sampling, while those for τ_{mob} and t^* are larger for $T \geq 0.9$ where DH is weak.

T	ρ	τ_{bond}	τ_χ	τ_α	τ_{ov}	τ_{imm}	τ_{mob}	t^*
1	0.933	2.7	0.52	0.24	1.2	1.6	1.2	0.84
0.9	1.016	3.6	0.76	0.29	1.8	2.0	0.88	0.88
0.8	1.085	5.5	1.2	0.37	2.6	2.4	1.2	1.0
0.75	1.116	7.2	1.6	0.42	3.3	3.2	1.4	1.2
0.7	1.147	10	2.2	0.49	4.2	3.8	1.4	1.3
0.65	1.177	15	3.2	0.60	5.7	4.6	1.6	1.6
0.6	1.206	24	5.2	0.80	8.8	6.4	2.0	2.2
0.55	1.235	42	9.4	1.2	16	11	3.2	3.2
0.525	1.248	62	14	1.6	24	15	4.4	4.2
0.5	1.263	1.0×10^2	23	2.4	38	24	5.4	6.4
0.49	1.269	1.3×10^2	29	2.9	48	25	7	7.2
0.48	1.274	1.7×10^2	38	3.7	63	38	8.4	9.4
0.47	1.280	2.2×10^2	51	5.0	87	57	11	13
0.46	1.285	3.1×10^2	73	7.3	1.3×10^2	66	15	15
0.45	1.291	4.7×10^2	1.2×10^2	12	2.0×10^2	1.1×10^2	22	23
0.44	1.297	7.5×10^2	1.9×10^2	21	3.3×10^2	1.9×10^2	29	34
0.43	1.302	1.3×10^3	3.3×10^2	49	6.2×10^2	3.5×10^2	56	60
0.42	1.308	2.7×10^3	6.9×10^2	1.2×10^2	1.4×10^3	9.9×10^2	99	96
0.41	1.314	6.4×10^3	1.7×10^3	3.4×10^2	3.6×10^3	2.8×10^3	2.7×10^2	1.9×10^2
0.4	1.319	2.0×10^4	5.6×10^3	1.5×10^3	1.3×10^4	1.3×10^4	8.3×10^2	4.6×10^2
0.39	1.325	7.4×10^4	2.2×10^4	7.0×10^3	5.5×10^4	4.4×10^4	3.1×10^3	9.4×10^2
0.38	1.330	3.2×10^5	9.9×10^4	3.7×10^4	2.6×10^5	3.2×10^5	9.7×10^3	3.0×10^3

We also find that s_{bond} is nearly T -independent; it remains below s_{ov} for all T , and is comparable to s_α for $T \lesssim T_x$. α relaxation and neighbor persistence being similarly spatially heterogeneous in this T regime is physically reasonable if both are controlled primarily by the immobile-particle clusters [11, 68].

Finally, Table I presents numerical values of the seven relaxation times discussed in Sec. IIIB. Note that these

times are likely to be substantially shorter than the corresponding times in the other recent study of the 2:1 KA model's dynamics at these T [74] because that study employed NVT -ensemble simulations performed at a fixed density $\rho = N/V = 1.4\sigma_{AA}^{-3}$ which is much larger than any of the densities considered here. The KA model's dynamics slow down rapidly with increasing pressure, particularly for low P [40, 59].

[1] M. D. Ediger, C. A. Angell, and S. R. Nagel, "Supercooled liquids and glasses," J. Phys. Chem. **100**, 13200

(1996).

[2] M. D. Ediger, "Spatially heterogeneous dynamics in su-

- percooled liquids,” *Ann. Rev. Phys. Chem* **51**, 99 (2000).
- [3] H. Sillescu, “Heterogeneity at the glass transition: a review,” *J. Non-Crystal. Solids* **243**, 81 (1999).
- [4] M. T. Cicerone and M. D. Ediger, “Relaxation of spatially heterogeneous dynamic domains in supercooled ortho-terphenyl,” *J. Chem. Phys.* **103**, 5684 (1995).
- [5] A. Heuer, M. Wilhelm, H. Zimmermann, and H. W. Spiess, “Rate memory of structural relaxation in glasses and its detection by multidimensional nmr,” *Phys. Rev. Lett.* **75**, 2851 (1995).
- [6] W. K. Kegel and A. von Blaaderen, “Direct observation of dynamical heterogeneities in colloidal hard-sphere suspensions,” *Science* **287**, 290 (2000).
- [7] W. Kob, C. Donati, S. J. Plimpton, P. H. Poole, and S. C. Glotzer, “Dynamical heterogeneities in a supercooled Lennard-Jones liquid,” *Phys. Rev. Lett.* **79**, 2827 (1997).
- [8] C. Donati, J. F. Douglas, W. Kob, S. J. Plimpton, P. H. Poole, and S. C. Glotzer, “Stringlike cooperative motion in a supercooled liquid,” *Phys. Rev. Lett.* **80**, 2338 (1998).
- [9] C. Donati, S. C. Glotzer, P. H. Poole, W. Kob, and S. J. Plimpton, “Spatial correlations of mobility and immobility in a glass-forming Lennard-Jones liquid,” *Phys. Rev. E* **60**, 3107 (1999).
- [10] N. Lacevic, F. W. Starr, T. B. Schroder, and S. C. Glotzer, “Spatially heterogeneous dynamics investigated via a time-dependent four-point density correlation function,” *J. Chem. Phys.* **119**, 7372 (2003).
- [11] F. W. Starr, J. F. Douglas, and S. Sastry, “The relationship of dynamical heterogeneity to the Adam-Gibbs and random first-order transition theories of glass formation,” *J. Chem. Phys.* **138**, 12A541 (2013).
- [12] L. Berthier, G. Biroli, J.-P. Bouchaud, L. Cipeletti, and W. van Saarloos, *Dynamical heterogeneities in glasses, colloids, and granular media* (Oxford University Press, 2011).
- [13] K. Paeng, H. Park, D. T. Hoang, and D. J. Kaufman, “Ideal probe single-molecule experiments reveal the intrinsic dynamic heterogeneity of a supercooled liquid,” *Proc. Natl. Acad. Sci. USA* **112**, 4952 (2015).
- [14] R. Richert, “Probing liquid dynamics, one molecule at a time,” *Proc. Nat. Acad. Sci. USA* **112**, 4841 (2015).
- [15] F. Puosi, A. Tripodo, M. Malvaldi, and D. Leporini, “Johari-Goldstein heterogeneous dynamics in a model polymer,” *Macromolecules* **54**, 2053 (2021).
- [16] X. Xu, J. F. Douglas, and W.-S. Xu, “Thermodynamic-dynamic interrelations in glass-forming polymer fluids,” *Macromolecules* **55**, 8699 (2022).
- [17] X. Wang, W.-S. Xu, H. Zhang, and J. F. Douglas, “Universal nature of dynamic heterogeneity in glass-forming liquids: A comparative study of metallic and polymeric glass-forming liquids,” *J. Chem. Phys.* **151**, 184503 (2019).
- [18] W. Zhang, J. F. Douglas, and F. W. Starr, “What does the instantaneous normal mode spectrum tell us about dynamical heterogeneity in glass-forming fluids?” *J. Chem. Phys.* **151**, 184904 (2019).
- [19] A. Giuntoli, F. Puosi, F. W. Starr, D. Leporini, and J. F. Douglas, “Predictive relation for the α -relaxation time of a coarse-grained polymer melt under steady shear,” *Sci. Adv.* **6**, eaaz0777 (2020).
- [20] L. Gao, H.-B. Yu, T. B. Schröder and J. C. Dyre, “Unified percolation scenario for the α and β processes in simple glass formers”, <https://arxiv.org/abs/2411.02922>.
- [21] J. Frenkel, *Kinetic Theory of Liquids* (Oxford University Press (Oxford), 1946).
- [22] A. Rahman, “Liquid structure and self-diffusion,” *J. Chem. Phys.* **45**, 2585 (1966).
- [23] J. C. Conrad, P. P. Dhillon, E. R. Weeks, D. R. Reichman, and D. A. Weitz, “Contribution of slow clusters to the bulk elasticity near the colloidal glass transition,” *Phys. Rev. Lett* **97**, 265701 (2006).
- [24] Z. Zhang, P. J. Yunker, P. Habdas, and A. G. Yodh, “Cooperative rearrangement regions and dynamical heterogeneities in colloidal glasses with attractive versus repulsive interactions,” *Phys. Rev. Lett.* **107**, 208303 (2011).
- [25] M. Laurati, P. Maßhoff, K. J. Mutch, S. U. Egelhaaf, and A. Zaccane, “Long-lived neighbors determine the rheological response of glasses,” *Phys. Rev. Lett.* **118**, 018002 (2017).
- [26] R. Higler, J. Krausseer, J. van der Gucht, A. Zaccane, and J. Sprakel, “Linking slow dynamics and microscopic connectivity in suspensions of charged colloids,” *Soft Matt.* **14**, 780 (2018).
- [27] J. C. Dyre, N. B. Olsen, and T. Christensen, “Local elastic expansion model for viscous-flow activation energies of glass-forming molecular liquids,” *Phys. Rev. B* **53**, 2171 (1996).
- [28] J. C. Dyre, “Colloquium: The glass transition and elastic models of glass-forming liquids,” *Rev. Mod. Phys.* **78**, 953 (2006).
- [29] R. Yamamoto and A. Onuki, “Dynamics of highly supercooled liquids: Heterogeneity, rheology, and diffusion,” *Phys. Rev. E* **58**, 3515 (1998).
- [30] H. Shiba, T. Kawasaki, and A. Onuki, “Relationship between bond-breakage correlations and four-point correlations in heterogeneous glassy dynamics: Configuration changes and vibration modes,” *Phys. Rev. E* **86**, 041504 (2012).
- [31] T. Iwashita, D. M. Nicholson, and T. Egami, “Elementary excitations and crossover phenomenon in liquids,” *Phys. Rev. Lett.* **110**, 205504 (2013).
- [32] C. Scalliet, B. Guiselin, and L. Berthier, “Thirty milliseconds in the life of a supercooled liquid,” *Phys. Rev. X* **12**, 041028 (2022).
- [33] J. C. Dyre, “Solid-that-flows picture of glass-forming liquids,” *J. Phys. Chem. Lett.* **15**, 1603 (2024).
- [34] W. Kob and H. C. Andersen, “Scaling behavior in the beta-relaxation regime of a supercooled Lennard-Jones mixture,” *Phys. Rev. Lett.* **73**, 1376 (1994).
- [35] W. Kob and H. C. Andersen, “Testing mode-coupling theory for a supercooled binary Lennard-Jones mixture. ii. intermediate scattering function and dynamic susceptibility,” *Phys. Rev. E* **52**, 4134 (1995).
- [36] R. S. Hoy and K. A. Interiano-Alberto, “Efficient d-dimensional molecular dynamics simulations for studies of the glass-jamming transition,” *Phys. Rev. E* **105**, 055305 (2022).
- [37] <http://labs.cas.usf.edu/softmattertheory/hdMD.html>.
- [38] T. S. Ingebrigtsen, J. C. Dyre, T. B. Schröder, and C. P. Royall, “Crystallization instability in glass-forming mixtures,” *Phys. Rev. X* **9**, 031016 (2019).
- [39] S. Sastry, “The relationship between fragility, configurational entropy and the potential energy landscape of glass-forming liquids,” *Nature* **279** (2001).
- [40] Q.-L. Yuan, X. Xu, J. F. Douglas, and W.-S. Xu, “In-

- fluence of density and pressure on glass formation in the Kob-Andersen model,” *J. Phys. Chem. B* **128**, 9889 (2024).
- [41] X. Wang, H. Zhang, and J. F. Douglas, “The initiation of shear band formation in deformed metallic glasses from soft localized domains,” *J. Chem. Phys.* **155**, 204504 (2021).
- [42] S. Karmakar, C. Dasgupta, and S. Sastry, “Growing length and time scales in glass-forming liquids,” *Proc. Natl. Acad. Sci.* **106**, 3675 (2009).
- [43] S. Karmakar, C. Dasgupta, and S. Sastry, “Analysis of dynamic heterogeneity in a glass former from the spatial correlations of mobility,” *Phys. Rev. Lett.* **105**, 015701 (2010).
- [44] E. Flenner and G. Szamel, “Dynamic heterogeneity in a glass forming fluid: Susceptibility, structure factor, and correlation length,” *Phys. Rev. Lett.* **105**, 217801 (2010).
- [45] K. Kim and S. Saito, “Multiple length and time scales of dynamic heterogeneities in model glass-forming liquids: A systematic analysis of multi-point and multi-time correlations,” *J. Chem. Phys.* **138**, 12A506 (2013).
- [46] D. S. Simmons and J. F. Douglas, “Nature and interrelations of fast dynamic properties in a coarse-grained glass-forming polymer melt,” *Soft Matt.* **7**, 11010 (2011).
- [47] W.-G. Zhang, J. F. Douglas, and F. W. Starr, “Effects of a “bound” substrate layer on the dynamics of supported polymer films,” *J. Chem. Phys.* **147**, 044901 (2017).
- [48] R. D. Mountain and D. Thirumalai, “Relationship between the fluctuation metric and the non-ergodicity parameter: incoherent scattering function,” *Physica A* **192**, 543 (1993).
- [49] S. Sastry, P. G. Debenedetti, S. Torquato, and F. H. Stillinger, “Signatures of distinct dynamical regimes in the energy landscape of a glass-forming liquid,” *Nature* **393**, 554 (1998).
- [50] U. Bengtzelius, W. Gotze, and A. Sjolander, “Dynamics of supercooled liquids and the glass-transition,” *J. Phys. C - Sol. State Phys.* **17**, 5915 (1984).
- [51] L. Berthier and G. Tarjus, “Critical test of the mode-coupling theory of the glass transition,” *Phys. Rev. E* **82**, 031502 (2010).
- [52] F. Stickel, E. W. Fischer, and R. Richert, “Dynamics of glass-forming liquids. ii. detailed comparison of dielectric relaxation, dc-conductivity, and viscosity data,” *J. Chem. Phys.* **104**, 2043 (1996).
- [53] F. W. Starr, F. Sciortino, and H. E. Stanley, “Dynamics of simulated water under pressure,” *Phys. Rev. E* **60**, 6757 (1999).
- [54] R. Casalini and C. M. Roland, “Scaling of the supercooled dynamics and its relation to the pressure dependences of the dynamic crossover and the fragility of glass formers,” *Phys. Rev. E* **71**, 014210 (2005).
- [55] J. Dudowicz and K. F. Freed, “Generalized entropy theory of polymer glass formation,” *Adv. Chem. Phys.* **137**, 125 (2008).
- [56] P. Crowther, F. Turci, and C. P. Royall, “The nature of geometric frustration in the Kob-Andersen mixture,” *J. Chem. Phys.* **143**, 044503 (2015).
- [57] J. F. Douglas and D. Leporini, “Obstruction model of the fractional stokes-einstein relation in glass-forming liquids,” *J. Non-Crystall. Solids* **235**, 137 (1998).
- [58] X. Xu, J. F. Douglas, and W.-S. Xu, “Parallel emergence of rigidity and collective motion in a family of simulated glass-forming polymer fluids,” *Macromolecules*, 4929 (2013).
- [59] Q.-L. Yuan, X. Xu, J. F. Douglas, and W.-S. Xu, “Understanding relaxation in the Kob-Andersen liquid based on entropy, string, shoving, localization, and parabolic models,” *J. Phys. Chem. B* **128**, 10999 (2024).
- [60] E. R. Weeks, J. C. Crocker, A. C. Levitt, A. Schofield, and D. A. Weitz, “Three-dimensional direct imaging of structural relaxation near the colloidal glass transition,” *Science* **287**, 627 (2000).
- [61] P. Chaudhuri, L. Berthier, and W. Kob, “Universal nature of particle displacements close to glass and jamming transitions,” *Phys. Rev. Lett.* **99**, 060604 (2007).
- [62] B. Wang, S. M. Anthony, S. C. Bae, and S. Granick, “Anomalous yet Brownian,” *Proc. Nat. Acad. Sci.* **106**, 15160 (2009).
- [63] B. Wang, J. Kuo, S. C. Bae, and S. Granick, “When Brownian diffusion is not Gaussian,” *Nat. Mat.* **11**, 481 (2012).
- [64] E. Barkai and S. Burov, “Packets of diffusing particles exhibit universal exponential tails,” *Phys. Rev. Lett.* **124**, 060603 (2020).
- [65] H. Zhang, C. Zhong, J. F. Douglas, X. Wang, Q. Cao, D. Zhang, and J.-Z. Jiang, “Role of string-like collective atomic motion on diffusion and structural relaxation in glass forming Cu-Zr alloys,” *J. Chem. Phys.* **142**, 164506 (2015).
- [66] A. Heuer, “Information content of multitime correlation functions for the interpretation of structural relaxation in glass-forming systems,” *Phys. Rev. E* **56**, 730 (1997).
- [67] E. Flenner and G. Szamel, “Lifetime of dynamic heterogeneities in a binary Lennard-Jones mixture,” *Phys. Rev. E* **70**, 052501 (2004).
- [68] H. Mizuno and R. Yamamoto, “Lifetime of dynamical heterogeneity in a highly supercooled liquid,” *Phys. Rev. E* **82**, 30501 (2010).
- [69] R. K. Pandit and H. E. Castillo, “Simple model for dynamic heterogeneity in glass-forming liquids,” *Phys. Rev. Lett.* **131**, 218202 (2023).
- [70] B. A. P. Betancourt, F. W. Starr, and J. F. Douglas, “String-like collective motion in the α - and β -relaxation of a coarse-grained polymer melt,” *J. Chem. Phys.* **148**, 104508 (2018).
- [71] H. Zhang, X. Wang, H.-B. Yu, and J.-F. Douglas, “Fast dynamics in a model metallic glass-forming material,” *J. Chem. Phys.* **154**, 084505 (2021).
- [72] C.-Y. Jiang, M. Baggioni, and J. F. Douglas, “Stringlet excitation model of the boson peak,” *J. Chem. Phys.* **160**, 214505 (2024).
- [73] P. Allegrini, J. F. Douglas, and S. C. Glotzer, “Dynamic entropy as a measure of caging and persistent particle motion in supercooled liquids,” *Phys. Rev. E* **60**, 5714 (1999).
- [74] L. Ortlieb, T. S. Ingebrigtsen, J. E. Hallett, F. Turci, and C. P. Royall, “Probing excitations and cooperatively rearranging regions in deeply supercooled liquids,” *Nature Comm.* **14**, 2621 (2023).